Compliant Yet Brittle Mechanical Behavior of Li_2S–P_2S_5 Lithium-Ion-Conducting Solid Electrolyte

*Frank P. McGrogan, Tushar Swamy, Sean R. Bishop, Erica Eggleton, Lukas Porz, Xinwei Chen, Yet-Ming Chiang, and Krystyn J. Van Vliet**

Li-ion batteries have provided compact, lightweight, and rechargeable energy storage, enabling a range of new technologies over more than two decades. Recently, the drive toward both safer and higher energy density storage has motivated an increasing focus on all-solid-state batteries, wherein the solid electrolyte is anticipated to preclude dendrite formation leading to electrical shorting and is furthermore nonflammable. If realized, these advantages could significantly improve battery safety and enable use of higher energy density electrodes.[1,2]

Crystalline and amorphous sulfide electrolytes (e.g., Li_2S–P_2S_5 or LPS) have now been widely reported to have Li-ion conductivity near room temperature that is high enough (>10^{-4} S cm^{-1}) to warrant consideration as the basis for a new class of solid-state batteries.[3–5] A key concern in these and other solid electrolytes, however, is their mechanical stability in the presence of strains in the adjacent electrode materials accompanying reversible Li storage (intercalation or alloying) that may vary from a few percent by volume up to a factor of three (e.g., in the case of silicon anodes).[6,7] Sulfide-based electrolytes have remarkably lower Young's modulus (≈20 GPa[8]) than many of these active materials (e.g., 100–200 GPa), as well as oxide-based solid electrolytes such as the garnets (100–200 GPa for $Li_7La_3Zr_2O_{12}$ or LLZO and $Li_{0.33}La_{0.57}TiO_3$ or LLTO[8–10]), which initially suggested to us that the sulfides might exhibit superior strain-accommodation characteristics in solid-state batteries. However, a detailed understanding of elastoplastic and fracture properties, which has heretofore been lacking, is required to draw clear conclusions of material design and selection for sulfide solid electrolytes.

Here, we used instrumented indentation to quantify three fundamental mechanical properties of an amorphous Li_2S–P_2S_5 (70:30 mol%) solid electrolyte prepared by a melt-quenching procedure: Young's elastic modulus E, hardness H, and fracture toughness K_{Ic}. Mechanical property characterization of the sulfide electrolytes is exceptionally challenging due to their extreme moisture sensitivity; exposure to air alone quickly degrades the sample surfaces. Therefore, we obtained E and H from instrumented indentation measurements within a specialized fluid cell that immersed the sample in mineral oil, a liquid medium that we found to be nonreactive with the sulfide electrolyte (**Figure 1**). We evaluated K_{Ic} via postindentation imaging of crack dimensions[11,12] through a protective mineral oil film. These measurements provide an improved understanding of sulfide electrolyte mechanical properties necessary for predictive modeling of elastic stress distributions and fracture conditions in solid-state battery structures.

The elastic modulus E and hardness H of amorphous LPS were measured to be 18.5 ± 0.9 GPa and 1.9 ± 0.2 GPa, respectively. The E of LPS is thus much lower than that reported for typical oxide glasses; for example, soda lime and borosilicate

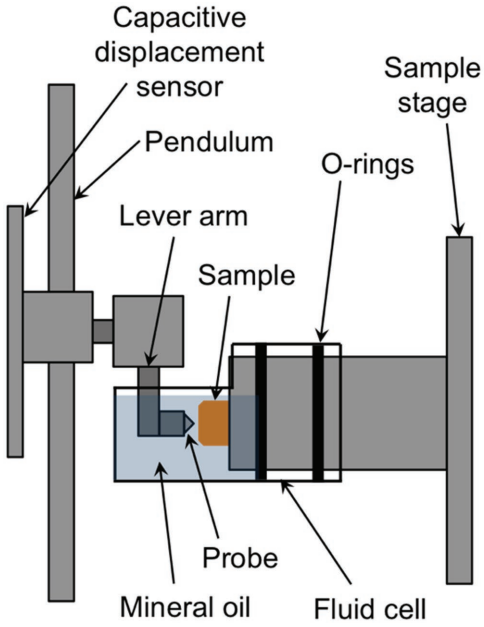

Figure 1. Schematic of liquid cell used to immerse the sulfide sample in mineral oil during instrumented indentation.

F. P. McGrogan, Dr. S. R. Bishop, E. Eggleton, L. Porz, Dr. X. Chen,[+] Prof. Y.-M. Chiang, Prof. K. J. Van Vliet
Department of Materials Science and Engineering
Massachusetts Institute of Technology
Cambridge, MA 02139, USA
E-mail: krystyn@mit.edu

T. Swamy
Department of Mechanical Engineering
Massachusetts Institute of Technology
Cambridge, MA 02139, USA

Dr. S. R. Bishop
Department of Nuclear Science and Engineering
Massachusetts Institute of Technology
Cambridge, MA 02139, USA

Prof. K. J. Van Vliet
Department of Biological Engineering
Massachusetts Institute of Technology
Cambridge, MA 02139, USA

[+]Present address: Institute of Materials Research and Engineering, Singapore 138634, Singapore

DOI: 10.1002/aenm.201602011

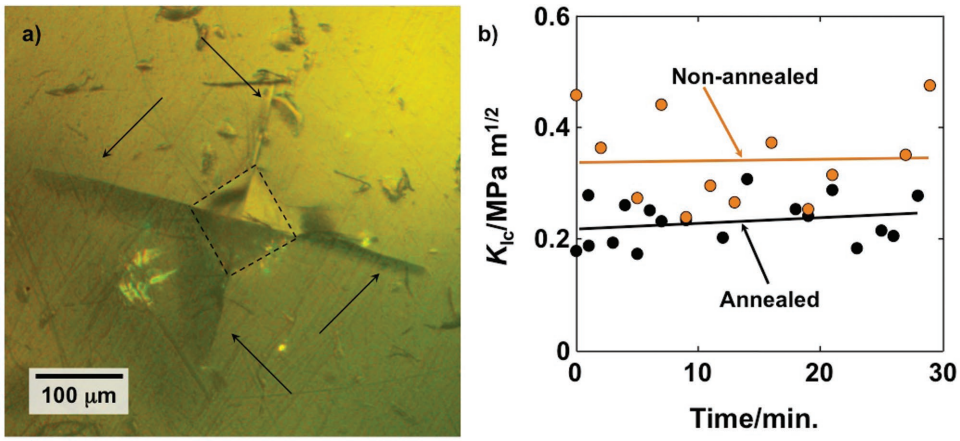

Figure 2. a) Fracture in the form of visible cracks (arrows) resulting from Vickers indentation (dashed diamond) load of ≈10 N on glassy Li_2S–P_2S_5 (LPS). b) K_{Ic} did not change detectably or steadily with time, for either the annealed or nonannealed samples, indicating stability of the LPS surface under mineral oil.

glasses have E of approximately 70 GPa.[13] This relatively low E also corresponds to a shear modulus of $G = 7.1 \pm 0.3$ GPa (assuming elastic isotropy and Poisson's ratio $\nu = 0.3$ as reported by Sakuda et al.[8]) that is sufficiently compliant to allow dendritic penetration of Li by the Monroe and Newman criterion.[9,14] The hardness H is at the low end of the range for oxide glasses, which varies from 2 to 8 GPa,[15] and at the high end of reported hardness for chalcogenide glasses, which ranges from 0.3 to 2 GPa.[15] Note that the hardness of LPS is similar to that of crystalline metallic alloys (e.g., aluminum 7075[16]) but about three orders of magnitude higher than that of pure alkali metals.[17]

Fracture toughness K_{Ic} as measured by crack length analysis (**Figure 2**a) was 0.23 ± 0.04 MPa m$^{1/2}$, more than a factor of two lower than oxide glasses such as soda lime and borosilicate glasses, which exhibit K_{Ic} in the range of 0.5–1.0 MPa m$^{1/2}$.[18] As discussed in the Experimental Section, an annealing step that heated the sample to slightly below the glass transition temperature was included to consider whether residual stresses from quenching significantly affected K_{Ic}. A second sample prepared without this annealing step was tested for comparison. The measured K_{Ic} of the non-annealed sample was 0.34 ± 0.08 MPa m$^{1/2}$, which was significantly higher than that measured for the annealed sample ($p < 0.001$, Welch's t-test). This statistically significant difference was modest (0.11 MPa m$^{1/2}$) and within a range that could be attributed to sample-to-sample variation, and thus this comparison demonstrates chiefly that annealing at 150 °C did not increase the effective K_{Ic} by relieving thermal stresses. K_{Ic} did not vary detectably as a function of time over the experimental duration (Figure 2b), indicating that the sample surface was chemically stable under mineral oil for these durations.

Note that the relatively low K_{Ic} measured for this solid electrolyte was comparable to that for delithiated Li_XCoO_2 cathode; upon delithiation, K_{Ic} of Li_XCoO_2 decreases from 0.94 to 0.25 MPa m$^{1/2}$, as we have reported previously.[19] As the data presented here are the first report of plastic and fracture properties of any sulfide solid electrolytes, these magnitudes provide a key baseline to test whether substantial variations exist in the LPS family as a function of composition or crystallinity. Thus, overall this solid electrolyte is elastically compliant with relatively low resistance to reversible deformation, while also brittle with low resistance to fracture. In comparison to LPS, solid polymer electrolytes are significantly more compliant ($E \approx 1$ MPa[20,21] to $E \approx 1$ GPa[22]) with typically higher fracture toughness ($K_{Ic} \approx 0.5$ MPa m$^{1/2}$).[22] Solid electrolyte garnet-type oxides such as LLTO and LLZO are much stiffer ($E \approx 100$ GPa), but likewise less brittle ($K_{Ic} \approx 0.9$–1.6 MPa m$^{1/2}$ when measured via Newton-scale indentation as reported herein).[10,23]

To confirm the structure and conductivity of the sample, we ground the LPS to a powder form and conducted X-ray diffraction (XRD) and electrochemical impedance spectroscopy (EIS) measurements. **Figure 3**a shows the XRD pattern of the melt-quenched LPS sample (after grinding to powder), the same material after annealing for stress relief, and the pattern reported by Minami et al.[24] for "glassy" LPS powder obtained via the same melt-quenching process. We observed broad peaks for the present samples indicating a high degree of disorder; the extent of short-range order or possibly nanocrystalline content requires a more detailed study, such as by pair-distribution function analysis. Direct observation by transmission electron microscopy and related methods is challenged by the extreme moisture sensitivity of these materials. However, as discussed below, the ionic conductivity of the present material is comparable to those reported previously for other LPS considered to be amorphous; specifically, the conductivity was reported to be somewhat lower for amorphous than for crystalline LPS,[24] and thus our samples are assumed to be similarly disordered.

Figure 3b shows EIS results from experiments conducted with stainless steel (SS) blocking electrodes (SS/LPS/SS, as shown in the inset) on the as-synthesized LPS powder, and after annealing at 150 °C for 5 h. The reproducible XRD and impedance spectra after annealing indicate that no further change in the structure occurred during this annealing step. The intercept with the horizontal axis at high frequency, indicated by the arrow in Figure 3b, is attributed to the bulk electrolyte resistance. Upon converting resistance to conductivity by accounting for the geometry of the sample, we obtain a room-temperature conductivity value of 3×10^{-4} S cm^{-1} for the as-synthesized LPS

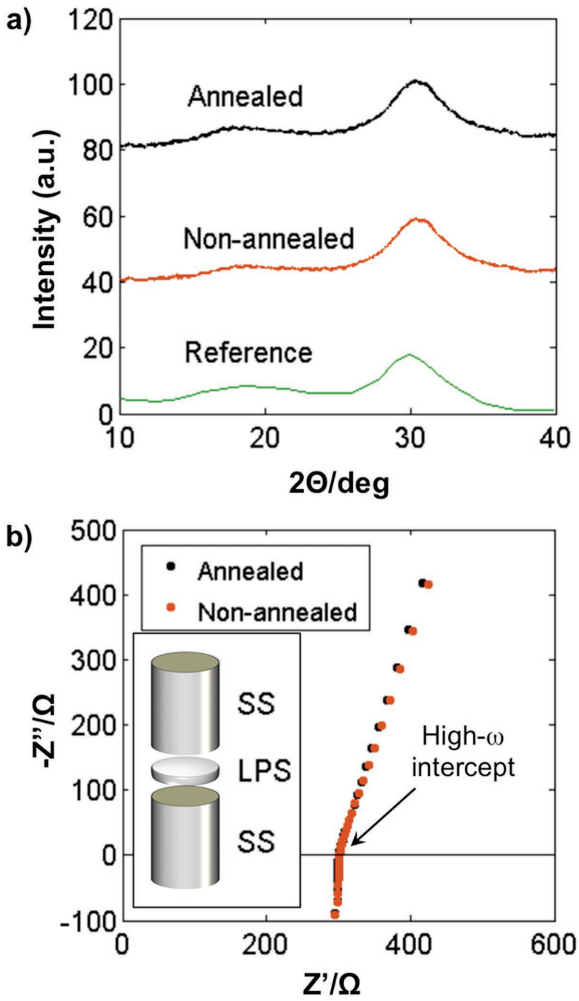

Figure 3. Characterization of Li_2S–P_2S_5 (LPS). a) X-ray diffraction pattern of the as-synthesized LPS powder, after annealing at 150 °C for 5 h, and reference pattern reproduced from Minami et al.[24] Absence of sharp peaks suggests a predominantly glassy or amorphous phase. b) Ionic conductivity data measured via EIS for SS/LPS/SS configuration in inset, where SS denotes stainless steel.

powder. This magnitude is consistent with other reports in the literature for amorphous LPS.[24]

To summarize the variation in mechanical properties that would typically be present in an all-solid-state lithium battery, we illustrate in **Figure 4** a simplified battery "stack" consisting of a Li_XCoO_2 cathode, LPS electrolyte, and Li metal anode, along with the corresponding E, H, and K_{Ic}. During cycling over typical capacity limits, Li_XCoO_2 is known to undergo ≈1.9% molar volume change,[19,25] while the lithium electrode will undergo an absolute volume change dictated by the amount of Li being reversibly transported. The relatively low E of LPS indicates that imposed strains, such as those incurred by cyclic expansion of an adjacent electrode, will be accommodated with less stress than for a high-modulus electrolyte such as a garnet. However, the low K_{Ic} of LPS also means that the brittle fracture could occur at lower stresses, depending on details of defect size and population. Note that even for this simplified stack, additional information such as the interfacial mechanical properties and defect population is necessary to predict modes of failure. However, the present results are a significant step toward understanding, modeling, and designing all-solid-state batteries for electro-chemomechanical reliability.

In conclusion, we determined the Young's modulus, hardness, and fracture toughness of glassy Li_2S–P_2S_5 solid electrolyte of 70:30 composition to be 18.5 ± 0.9 GPa, 1.9 ± 0.2 GPa, and 0.23 ± 0.04 MPa $m^{1/2}$, respectively, via indentation-based methods that maximized phase stability of the LPS sample. These results show that this LPS material—and by inference other solid electrolytes in the solid sulfide family—are distinguished as compliant yet significantly more brittle than crystalline oxide electrolytes considered for the same applications. Although the low stiffness of LPS suggests a capability of this solid electrolyte material to accommodate elastic mismatch with adjacent phases such as storage electrodes and current collectors in a solid-state battery, this capability is compromised by the low fracture toughness and corresponding high sensitivity to preexisting or cycling-generated flaws.

Experimental Section

Sample Preparation: Li_2S (99.9%; Alfa Aesar) and P_2S_5 (99%; Sigma-Aldrich) were mixed at a ratio of 70/30 mol% in an argon-filled glovebox and placed inside a carbon-coated quartz ampoule, which was then sealed under house vacuum. The sealed ampoule was placed in a preheated furnace at 750 °C for 2 h, followed by quenching in ice water to obtain the glassy LPS solid electrolyte. To remove thermal stresses that could affect the measurements, the quenched sample was annealed at 150 °C for 5 h, well below the glass transition temperature of ≈220 °C.[26]

To obtain polished samples for mechanical characterization, the solid sample of millimeter-scale thickness was mounted to a stainless steel spacer (via low-viscosity cyanoacrylate) within an argon-filled glovebox and attached to a hand-operated polishing tool. The sample was then polished in the glovebox using silicon carbide sandpaper of decreasing grit size (120, 500, 800, 1200, 2400, and 4000) and diamond polishing pads (3, 1, and 0.5 µm; UltraPrep, Beuhler Limited, Lake Bluff, IL). Tetrahydrofuran (anhydrous, >99.9% purity; Sigma-Aldrich) was used to rinse the sample and polishing tool after each polishing step, as it was observed to be nonreactive with the sample and other experimental components.

The LPS powder for conductivity samples and XRD measurements was obtained by first manually grinding a quenched/annealed solid sample, and then ball milling for 100 min in a SPEX SamplePrep Mixer/Mill 8000 M.

Phase and Electrochemical Characterization: The XRD pattern of the as-synthesized LPS solid electrolyte powder was obtained using a PANalytical X'Pert Pro multipurpose diffractometer equipped with a Cu Kα radiation source and an X'Celerator detector. The LPS powder was cold pressed in a 1.3 cm polycarbonate tube at 360 MPa between two SS current collectors to a thickness of ≈1 mm, preparing an SS/LPS/SS cell. EIS measurements were conducted at room temperature using a Solartron 1400/1470E cell test system, wherein the sinusoidal voltage amplitude was set to 10 mV and the frequency was swept from 1 MHz to 1 Hz.

Mechanical Characterization: To measure E and H via instrumented indentation, flat and polished LPS samples were mounted within a fluid cell designed specifically for use in a commercial, instrumented indenter (MicroMaterials, LLC, Wrexham, UK), as shown in Figure 1, and filled with mineral oil (Alfa Aesar). In this design, a lever arm is attached to the indentation pendulum and submerged in the liquid cell, so that all measurements take place with the sample and indenter immersed fully in the liquid medium.[27,28] Calibrations were conducted using the instrument software to account for any additional frame compliance

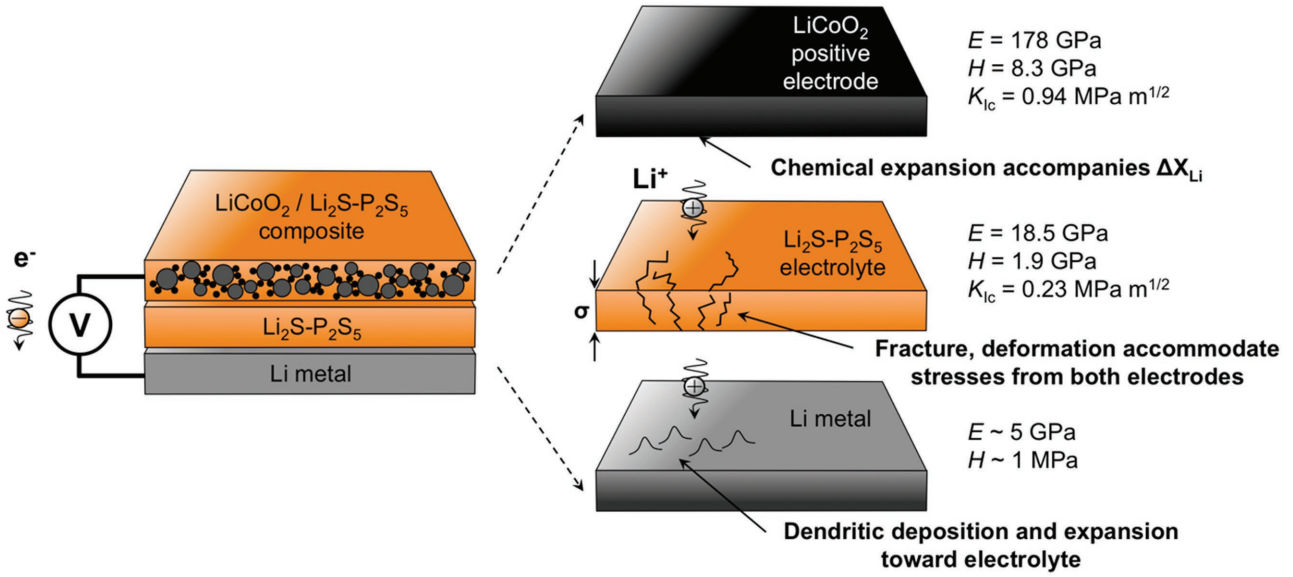

Figure 4. Summary of Li_2S–P_2S_5 (LPS) mechanical property data in the context of the all-solid-state batteries. While relatively low stiffness would enable strain accommodation from a composite Li_XCoO_2 cathode, low fracture toughness indicates high susceptibility to fracture and passage of Li dendrites. Data for Li_XCoO_2 is taken from Swallow et al.[19] and *E* and *H* Li estimates are based on Samsonov;[17] fracture toughness of Li is not reported to our knowledge.

(i.e., displacement of the instrument itself under applied load to the sample) that was introduced by the lever arm.

To ensure that the sample was not exposed to air (specifically moisture) during the entire mounting and measurement process, the sample mounting was conducted in an argon-filled glovebox (less than 10 ppm H_2O and 1 ppm O_2), and the liquid cell was filled with mineral oil therein. The liquid cell was then transferred from the glovebox to the instrumented indenter and carefully mounted in the instrument to maintain full sample immersion. The sample did not exhibit any visible changes in color or opacity throughout the indentation experiment, which is in stark contrast to a surface reaction forming a white crust on the sulfide that is otherwise observed upon <5 min of exposure to ambient air. (Gas purging to produce a dry environment within the testing chamber was less successful in preserving sample surface integrity over the experiment durations due to the high-moisture sensitivity of such materials.)

Mechanical properties of *E* and *H* were measured at 39 distinct sample surface locations ($n = 39$ indentations, comprising a rectangular grid of 4 × 10 replicate load–displacement profiles with one fiduciary marker in the corner of the grid) in this liquid cell configuration. A diamond probe of cube-corner geometry was used with load–depth hysteresis acquired up to a maximum load of 20 mN, resulting in maximum depths that were ≈2 µm and thus approximately three orders of magnitude less than the millimeter-scale sample thickness, such that finite-thickness effects were reasonably neglected. Data were acquired over a period of 120 s loading and 30 s unloading, with an intermediate dwell time at maximum load of 10 s. Center-to-center spacing of the indentations was 70 µm. Since indentation depths were typically ~2 µm, and therefore well beyond the probe apex, an ideal cube corner area function was used for subsequent data analysis.

From the load–depth hysteresis, reduced elastic moduli E_r were calculated using Equation (1),[29,30] wherein dP/dh represents the initial elastic response upon unloading

$$E_r = \frac{\sqrt{\pi}}{2}\frac{1}{\sqrt{A}}\frac{dP}{dh} \tag{1}$$

and *P*, *h*, and *A* correspond to the measured load, measured displacement, and calculated projected indentation area, respectively. The material Young's modulus *E* was calculated from E_r by accounting for the elastic properties of the diamond indenter,[31] as shown in Equation (2):

$$E = \frac{1-\upsilon^2}{\frac{1}{E_r}-\frac{1-\upsilon_i^2}{E_i}} \tag{2}$$

where E_i and Poisson's ratio ν_i of the diamond indenter were taken to be 1070 GPa and 0.07, respectively; Poisson's ratio ν of the sample was assumed as 0.3, as experimentally determined by Sakuda et al.[8] Hardness *H* was calculated as in Equation (3), where P_{max} is the maximum applied load:

$$H = \frac{P_{max}}{A} \tag{3}$$

Fracture toughness K_{Ic} can be quantified for brittle materials, including solid Li-intercalating electrodes, via direct measurement of sudden displacement excursions or "pop-ins" extending several nanometers during instrumented indentation.[19,32,33] However, these LPS solid electrolyte samples did not exhibit detectable displacement excursions associated with radial cracking under our accessible instrumented indentation conditions. Thus, we conducted microindentation with a diamond Vickers probe geometry (LECO LM248AT; Saint Joseph, MI) to apply Newton-scale loads to the material. The sample was not immersed within oil during such experiments due to instrument constraints. However, the surfaces of samples removed from mineral oil baths immediately before testing retained an oil surface film and thus remained stable for 15–30 min as required for these experiments. Beyond such durations, visible oxidation reaction products were apparent in some surface regions. Indentations were conducted only on pristine regions of the surface, and optical images were acquired through the oil film immediately before and after the indentations. Applied load of 1000 gf (9.8 N) with the Vickers probe using a dwell time of 15 s regularly resulted in the formation of radial cracks, typically from all four corners of the indentation, as shown in Figure 2a. Replicate data were collected on a quenched/annealed LPS sample ($n = 18$ measurements) and on a quenched/nonannealed LPS sample ($n = 12$) to investigate the possible effects of residual thermal stress on the measurement.

Estimation of K_{Ic} from radial cracks uses the crack length c, measured optically from the center of the indentation to the crack tip. Taking E and H as the values determined by the prior instrumented indentation hysteresis experiments, K_{Ic} was calculated using Equation (4)

$$K_{Ic} = k\left(\frac{E}{H}\right)^{1/2}\frac{P}{c^{3/2}} \quad (4)$$

where P is the applied load equal to 9.81 N and k is a constant taken to be 0.016 for the Vickers probe geometry.[12] We note that this approach provides a measure of K_{Ic} that is accessible to small sample geometries which, though quantified thus and reported for other brittle materials, is best considered as an approximation of the plane strain, Mode I tensile fracture toughness.

All mechanical property data were reported as mean ± standard deviation. For comparing means obtained with different variances and sample sizes n, the Welch's t-test was used to identify differences with statistical significance.

Acknowledgements

The authors gratefully acknowledge support from the US Department of Energy's Office of Basic Energy Science for the Chemomechanics of Far-From-Equilibrium Interfaces (COFFEI) small group, through award number DE-SC0002633 (J. Vetrano, Program Manager). This work made use of the DMSE Metlab (Laboratory for Physical Metallurgy) at MIT (Meri Treska, Senior Lecturer). The authors also acknowledge use of the MIT Nanomechanical Technology Laboratory (A. Schwartzman, Manager).

Received: September 9, 2016
Revised: November 18, 2016
Published online: January 30, 2017

[1] K. Takada, *Acta Mater.* **2013**, *61*, 759.
[2] J. Li, C. Ma, M. Chi, C. Liang, N. J. Dudney, *Adv. Energy Mater.* **2015**, *5*, 1401408.
[3] N. Kamaya, K. Homma, Y. Yamakawa, M. Hirayama, R. Kanno, M. Yonemura, T. Kamiyama, Y. Kato, S. Hama, K. Kawamoto, A. Mitsui, *Nat. Mater.* **2011**, *10*, 682.
[4] Z. Liu, W. Fu, E. A. Payzant, X. Yu, Z. Wu, N. J. Dudney, J. Kiggans, K. Hong, A. J. Rondinone, C. Liang, *J. Am. Chem. Soc.* **2013**, *135*, 975.
[5] Y. Seino, T. Ota, K. Takada, A. Hayashi, M. Tatsumisago, *Energy Environ. Sci.* **2014**, *7*, 627.
[6] W. H. Woodford, W. C. Carter, Y.-M. Chiang, *Energy Environ. Sci.* **2012**, *5*, 8014.
[7] S. R. Bishop, D. Marrocchelli, C. Chatzichristodoulou, N. H. Perry, M. B. Mogensen, H. L. Tuller, E. D. Wachsman, *Annu. Rev. Mater. Res.* **2014**, *44*, 205.
[8] A. Sakuda, A. Hayashi, Y. Takigawa, K. Higashi, M. Tatsumisago, *J. Ceram. Soc. Jpn.* **2013**, *121*, 946.
[9] S. Yu, R. D. Schmidt, R. Garcia-Mendez, E. Herbert, N. J. Dudney, J. B. Wolfenstine, J. Sakamoto, D. J. Siegel, *Chem. Mater.* **2016**, *28*, 197.
[10] Y.-H. Cho, J. Wolfenstine, E. Rangasamy, H. Kim, H. Choe, J. Sakamoto, *J. Mater. Sci.* **2012**, *47*, 5970.
[11] D. S. Harding, W. C. Oliver, G. M. Pharr, *Mater. Res. Soc. Symp. Proc.* **1995**, *356*, 663.
[12] G. R. Anstis, P. Chantikul, B. R. Lawn, D. B. Marshall, *J. Am. Ceram. Soc.* **1981**, *64*, 533.
[13] *Materials Data Book*, Cambridge University Engineering Department, Cambridge, UK **2003**.
[14] C. Monroe, J. Newman, *J. Electrochem. Soc.* **2005**, *152*, A396.
[15] J. E. Shelby, *Introduction to Glass Science and Technology*, Royal Society of Chemistry, Cambridge, UK, **2005**.
[16] T. A. Venkatesh, K. J. Van Vliet, A. E. Giannakopoulos, S. Suresh, *Scr. Mater.* **2000**, *42*, 833.
[17] G. V Samsonov, in *Handbook of the Physicochemical Properties of the Elements* (Ed: G. V. Samsonov), Springer, New York, NY **1968**, pp. 387–446.
[18] K. K. Ray, A. K. Dutta, *Br. Ceram. Trans.* **1999**, *98*, 165.
[19] J. G. Swallow, W. H. Woodford, F. P. McGrogan, N. Ferralis, Y.-M. Chiang, K. J. Van Vliet, *J. Electrochem. Soc.* **2014**, *161*, F3084.
[20] D. R. MacFarlane, J. Sun, P. Meakin, P. Fasoulopoulos, J. Hey, M. Forsyth, *Electrochim. Acta* **1995**, *40*, 2131.
[21] S. Ramesh, T. Winie, A. K. Arof, *Eur. Polym. J.* **2007**, *43*, 1963.
[22] D. H. Builes, J. P. Hernandez-Ortiz, M. A. Corcuera, I. Mondragon, A. Tercjak, *ACS Appl. Mater. Interfaces* **2014**, *6*, 1073.
[23] J. Wolfenstine, H. Jo, Y.-H. Cho, I. N. David, P. Askeland, E. D. Case, H. Kim, H. Choe, J. Sakamoto, *Mater. Lett.* **2013**, *96*, 117.
[24] K. Minami, A. Hayashi, M. Tatsumisago, *J. Ceram. Soc. Jpn.* **2010**, *118*, 305.
[25] J. N. Reimers, J. R. Dahn, *J. Electrochem. Soc.* **1992**, *139*, 2091.
[26] K. Minami, F. Mizuno, A. Hayashi, M. Tatsumisago, *Solid State Ionics* **2007**, *178*, 837.
[27] G. Constantinides, Z. I. Kalcioglu, M. McFarland, J. F. Smith, K. J. Van Vliet, *J. Biomech.* **2008**, *41*, 3285.
[28] B. Qing, K. J. Van Vliet, *Mol. Syst. Des. Eng.* **2016**, *1*, 290.
[29] W. C. Oliver, G. M. Pharr, *J. Mater. Res.* **1992**, *7*, 1564.
[30] W. C. Oliver, G. M. Pharr, *J. Mater. Res.* **2004**, *19*, 3.
[31] A. C. Fischer-Cripps, *Nanoindentation*, Springer, New York, NY **2002**.
[32] J. S. Field, M. V. Swain, R. D. Dukino, *J. Mater. Res.* **2003**, *18*, 1412.
[33] M. Qu, W. H. Woodford, J. M. Maloney, W. C. Carter, Y.-M. Chiang, K. J. Van Vliet, *Adv. Energy Mater.* **2012**, *2*, 940.

